AWARD NUMBER: **W81XWH-15-1-0341**

TITLE: **High Spatiotemporal Resolution Prostate MRI**

PRINCIPAL INVESTIGATOR: **Stephen J. Riederer, Ph.D.**

CONTRACTING ORGANIZATION: **Mayo Clinic**
Rochester, MN 55905

REPORT DATE: **September 2017**

TYPE OF REPORT: **Annual**

PREPARED FOR: U.S. Army Medical Research and Materiel Command
Fort Detrick, Maryland 21702-5012

REPORT DOCUMENTATION PAGE

Form Approved
OMB No. 0704-0188

1. REPORT DATE	**2. REPORT TYPE**	**3. DATES COVERED**
September 2017	Annual	15 Aug 2016 - 14 Aug 2017

4. TITLE AND SUBTITLE

High Spatiotemporal Resolution Prostate MRI

5a. CONTRACT NUMBER

5b. GRANT NUMBER
W81XWH-15-1-0341

5c. PROGRAM ELEMENT NUMBER

6. AUTHOR(S)

Stephen J. Riederer

E-Mail: Riederer@mayo.edu

5d. PROJECT NUMBER

5e. TASK NUMBER

5f. WORK UNIT NUMBER

7. PERFORMING ORGANIZATION NAME(S) AND ADDRESS(ES)

Mayo Clinic
200 1st ST SW
Rochester, MN 55905-0002

8. PERFORMING ORGANIZATION REPORT NUMBER

9. SPONSORING / MONITORING AGENCY NAME(S) AND ADDRESS(ES)

U.S. Army Medical Research and Materiel Command
Fort Detrick, Maryland 21702-5012

10. SPONSOR/MONITOR'S ACRONYM(S)

11. SPONSOR/MONITOR'S REPORT NUMBER(S)

12. DISTRIBUTION / AVAILABILITY STATEMENT

Approved for Public Release; Distribution Unlimited

13. SUPPLEMENTARY NOTES

14. ABSTRACT

Prostate cancer (PCa) is the second leading cause of cancer death in men. However, when detected and treated promptly the five-year relative survival rate approaches 100%. The overall purpose of this project is to develop improved means using MRI for detecting prostate cancer with the potential for differentiating disease aggressiveness. The hypothesis is that dynamic whole-volume contrast-enhanced perfusion imaging of the prostate gland can be performed with 1 mm isotropic spatial resolution and 2 sec frame times, providing an order of magnitude improvement over current techniques. The specific aims are: (i) to develop an MRI acquisition technique for time-resolved 3D MRI of the prostate, (ii) to develop a fundamentally new coil element family having variable sensitivity along the superior-to-inferior direction, (iii) to incorporate partial Fourier and acceleration methods into high speed reconstruction to provide high quality 3D images in real time at frame times of 2 sec or less.

15. SUBJECT TERMS

Prostate Cancer, Dynamic-Contrast-Enhanced Prostate MRI

16. SECURITY CLASSIFICATION OF:			**17. LIMITATION OF ABSTRACT**	**18. NUMBER OF PAGES**	**19a. NAME OF RESPONSIBLE PERSON** USAMRMC
a. REPORT	**b. ABSTRACT**	**c. THIS PAGE**			**19b. TELEPHONE NUMBER** ***(include area code)***
Unclassified	Unclassified	Unclassified	Unclassified	**20**	

TABLE OF CONTENTS

1. INTRODUCTION

Prostate cancer (PCa) is the second leading cause of cancer death in men after lung cancer. Approximately one in nine men will be diagnosed with prostate cancer but when detected early and treated promptly the five-year relative survival rate approaches 100%. The motivation of this project is to develop improved means for detecting prostate cancer. Magnetic resonance imaging (MRI) has been applied to the imaging of prostate cancer for several decades. The typical MRI prostate exam today consists of several "pulse sequences:" (i) T2-weighted spin-echo imaging; (ii) diffusion-weighted imaging (DWI); (iii) dynamic contrast-enhanced (DCE) perfusion MRI. While prostate cancer can be visualized using each sequence, only sequence (iii) provides dynamic information about the temporal enhancement pattern of any PCa lesions. The purpose of this project is to develop 10× improved spatiotemporal resolution DCE-MRI of prostate.

2. KEYWORDS

CAPR	Cartesian Acquisition with Projection Reconstruction-like sampling
CE-MRA	Contrast-Enhanced Magnetic Resonance Angiography
DCE-MRI	Dynamic-Constrast-Enhanced Magnetic Resonance Imaging
MRI	Magnetic Resonance Imaging
PCa	Prostate Cancer
SENSE	Sensitivity Encoding (a type of MRI acceleration technique)
SNR	Signal-to-Noise Ratio

3. ACCOMPLISHMENTS:

What were the major goals of the project?

Tasks for Months 1-21 (encompassing August 15, 2015 through June 1, 2017) taken from the grant application Statement of Work are shown below. Completed tasks reported in last year's report (July 2016) are shown with the month of completion in **blue (in parentheses)**. All tasks newly completed since then and reported here are shown with the completion month shown in **red (in parentheses)**.

Specific Aim 1: Development of MRI Acquisition Method	**Months**	**Investigator**
Major Task 1: Optimization of pCAPR Pulse Sequence Applied to Prostate Imaging		
Subtask 1.1: Determine parameter options for various spatiotemporal resolution combinations	1-6 **(5)**	Dr. Riederer; Dr. Kawashima; Mr. Borisch
Subtask 1.2: Design, construct, and test phantom which mimics geometry for prostate MRI	1-6 **(6)**	Dr. Riederer; Mr. Hulshizer
Subtask 1.3: Experimentally test and evaluate versions of pulse sequence with prostate phantom and select optimum sequence with standard receiver coil array	6-12 **(9,ongoing)** **(12)**	Dr. Riederer; Mr. Hulshizer
Subtask 1.4: Apply initial optimized pulse sequence to three volunteers with standard receiver coil array	13-15 **(15)**	Dr. Riederer; Dr. Kawashima

Subtask 1.5: Experimentally test and evaluate pulse sequence and triangular array with prostate phantom and select optimum sequence	16-24 **(20)**	Dr. Riederer; Mr. Hulshizer
Subtask 1.6: Determine parameter options for pulse sequence using prototype triangular coil array	18-24 **(20, ongoing)**	Dr. Riederer; Mr. Borisch
Specific Aim 2: Development of Special Purpose Receiver Coil Arrays		
Major Task 2: Optimization of pCAPR Pulse Sequence Applied to Prostate Imaging		
Subtask 2.1: Select optimum triangular element size and construct matched single pair of coils	1-6 **(3)**	Dr. Riederer; Mr. Hulshizer
Subtask 2.2: Construct, tune, and match multiple pairs of triangular coils	7-12 **(9)**	Dr. Riederer; Mr. Hulshizer
Subtask 2.3: Test modular triangular coil element prototype array with up to 16 elements (8 coil pairs) in experimental phantom studies	13-18 **(18)**	Dr. Riederer; Mr. Hulshizer
Specific Aim 3: Formation of Optimized pCAPR Images		
Major Task 3.1: Image Reconstruction and System Integration		
Subtask 3.1: Allowance for arbitrary acceleration factors (R_Y,R_Z) and CAIPIRINHA kernels for arbitrary R	1-6 **(6)**	Mr. Borisch
Subtask 3.2: Incorporate pCAPR pulse sequence into image reconstruction framework	7-12 **(7)**	Mr. Borisch
Subtask 3.3: Implement multi-processor execution of individual modules of reconstruction process	12-24 **(18)**	Mr. Borisch

What was accomplished under these goals?
The grant activities were subdivided into three specific aims with subtasks for each. Progress has been made for each aim. The following paragraphs are associated with the specific subtasks identified in the Statement of Work (SOW).

Specific Aim 1

Subtask 1.3. Work on this subtask continued since the time of last year's progress report. The phantom previously developed was further modified to include several simulated lesions within the inclusion simulating the prostate. A sagittal MR image of the phantom is shown in **Figure 1**. The overall size of the phantom simulates a patient of an approximate BMI of 23. A larger phantom is also being constructed. Related to this we have studied the effect of temporal resolution on the fidelity with which perfusion parameters are estimated. This was done by starting with the data acquired at 6.5 sec frame time and down sampling; i.e. taking every other point or possibly every third point Results similar to those in **Figure 2** show that temporal sampling coarser than the 6.5 sec used in this work causes underestimation of perfusion parameters.

Subtask 1.4. This subtask involved use of the optimized pulse sequence in three volunteers

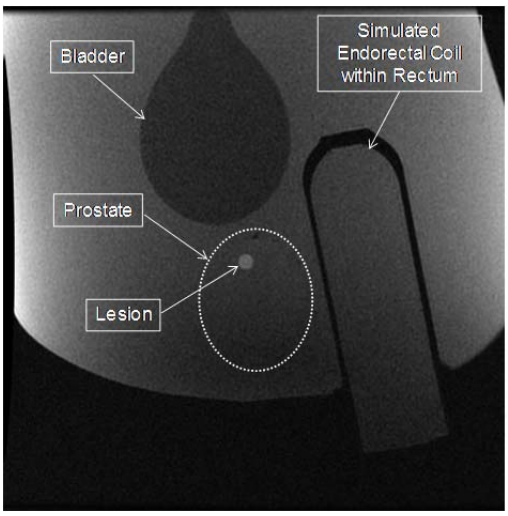

Figure 1. Sagittal MR image of prostate phantom with simulated lesion.

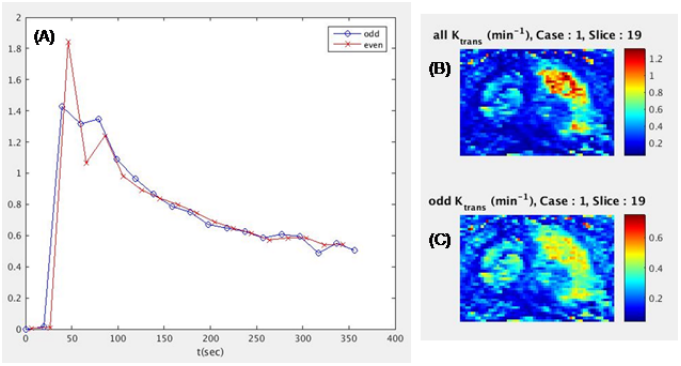

Figure 2. Plot illustrating (A) downsampled even and odd time points and maps of Ktrans using all data (6.5 sec) (B) and only the odd timepoints (C). The latter markedly causes underestimation of Ktrans.

using the standard receiver coil array. The principal target group of patients is that which is "treatment-naïve" in that prostate cancer is suspected but the presence or degree of disease must be determined prior to determination of possible treatment. The optimum sequence was identified in the first year, and for such patients temporal sampling the realm of 5 to 7 seconds represented a good tradeoff between spatial and temporal resolution. Volunteers have been imaged using the standard 12-element receiver coil array, and in fact this has been expanded to include studies of patients who are referred for prostate MRI. Further, we have studied to possible extension of the acquisition to include more, specifically 32, of the multicoil elements available. These additional elements are generally positioned more lateral than the reference 12 elements. For the same scan, use of 32 elements consistently provides improved image quality. Sample results are shown in **Figure 3**, and we have published these findings.

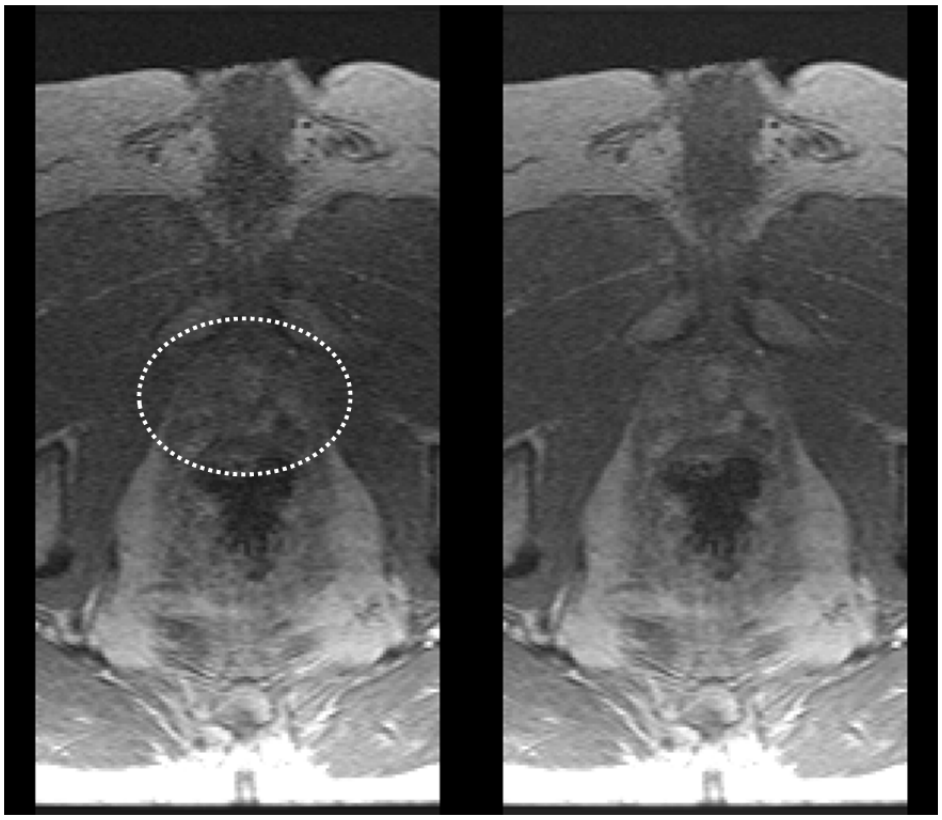

Figure 3. Comparison of images of the prostate acquired using 12-element standard coil (left) and 32-element coil (right). Prostate is identified within the dashed ellipse. The right image has superior signal-to-noise ratio.

Subtask 1.5. For this task we used a 12-element array composed of the new triangular elements

and imaged a prostate phantom to assess performance using the target prostate perfusion pulse sequence. Sample results are shown in **Figure 4**. This figure shows maximum intensity projection (MIP) images of the g-factor, a measure of the noise amplification of the coil array for sagittal (A), coronal (B) and axial (C) orientations. Also shown in (D) is the cumulative g-factor as measured over the 3D volume being imaged. This work is ongoing, and further measurements and comparisons will be made with the standard receiver coil.

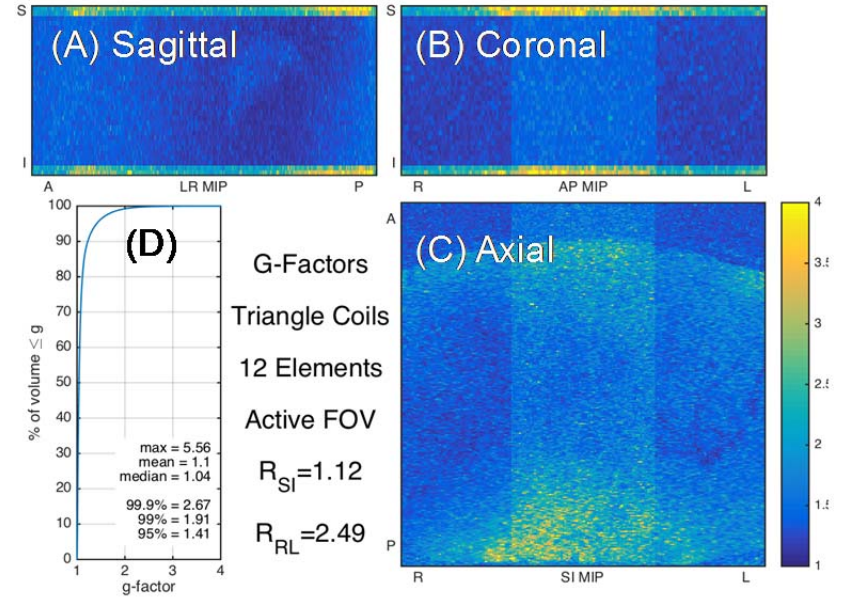

Figure 4. Plot of g-factors for 12-element coil composed of triangular elements.

Specific Aim 2

Subtask 2.3. The results in Figure 3 were generated using a 12-element coil. As specified in this subtask, we have further constructed a 16-element coil composed of the triangular elements. The design using two-element modules allows the total number of elements to be matched to the body habitus, i.e. patient diameter. A photograph of the 16-element coil is shown in **Figure 5**.

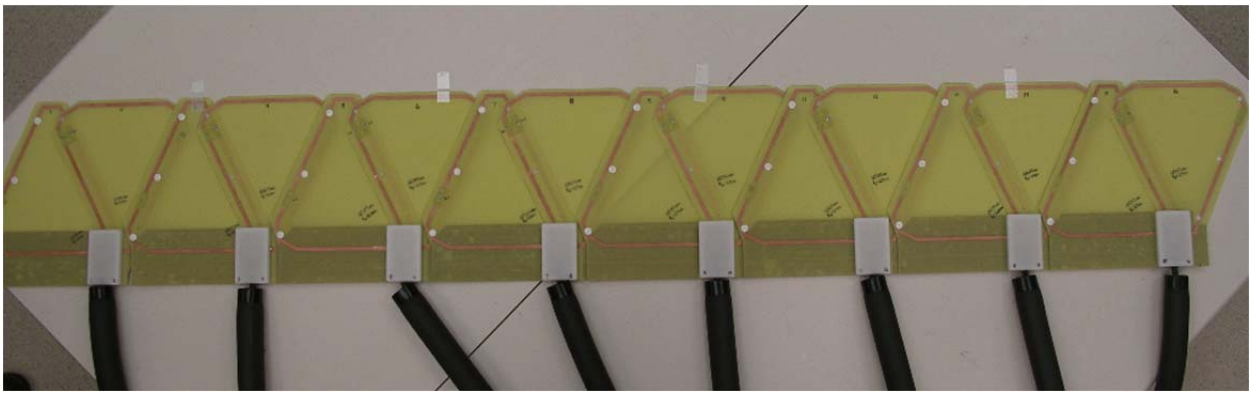

Figure 5. Photograph of 16-element coil composed of triangular elements.

Specific Aim 3

Subtask 3.3. The reconstruction hardware was identified last year and is shown in Figure 6. We have made progress on this aim and have updated the hardware to include two CPU packages, each with 14 physical cores and 28 threads, and thus a total of 28 cores (processor elements) and 56 threads. This routinely allows fast, clinically acceptable reconstruction times of 3D time-resolved, multi-coil (32 element) accelerated images of dynamic-contrast-enhanced (DCE) MRI. Each of the steps in the reconstruction (determination of coil sensitivities, Fourier transformation of raw data, un-aliasing of reconstructed images, presentation into 3D time series, conversion to vendor-compatible format) comprises an individual module.

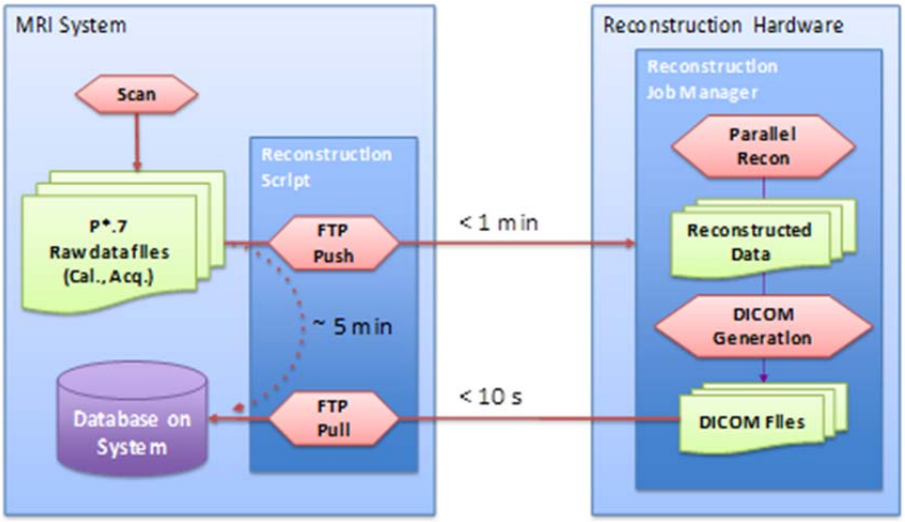

Figure 6. Schematic showing host MRI scanner (left) and custom computation hardware (right).

What opportunities for training and professional development has the project provided?
Nothing to report.

How were the results disseminated to communities of interest?
Nothing to report other than that in Section 6 of this report.

What do you plan to do during the next reporting period to accomplish the goals?
We will continue our work according to the tasks shown in the original Statement of Work.

4. **IMPACT:** Describe distinctive contributions, major accomplishments, innovations, successes, or any change in practice or behavior that has come about as a result of the project relative to:

What was the impact on the development of the principal discipline(s) of the project?
The tasks completed in the first 21 months of this three-year project provide a good basis for ongoing work for all three Aims in the months ahead.

What was the impact on other disciplines?
Nothing to Report

What was the impact on technology transfer?
Our baseline DCE-MRI pulse sequences are now used clinically at Mayo Clinic, both in Rochester and at Mayo Clinic Arizona. This is approximately ten patient studies per day.

What was the impact on society beyond science and technology?
Nothing to Report

5. **CHANGES/PROBLEMS:** The PD/PI is reminded that the recipient organization is required to obtain prior written approval from the awarding agency grants official whenever there are significant changes in the project or its direction. If not previously reported in writing, provide the following additional information or state, "Nothing to Report," if applicable:

Changes in approach and reasons for change
Nothing to Report

Actual or anticipated problems or delays and actions or plans to resolve them
Nothing to Report

Changes that had a significant impact on expenditures
Nothing to Report

Significant changes in use or care of human subjects, vertebrate animals, biohazards, and/or select agents

Significant changes in use or care of human subjects
Nothing to Report

Significant changes in use or care of vertebrate animals
Nothing to Report

Significant changes in use of biohazards and/or select agents
Nothing to Report

6. **PRODUCTS:** List any products resulting from the project during the reporting period. If there is nothing to report under a particular item, state "Nothing to Report."

- **Publications, conference papers, and presentations**
  Report only the major publication(s) resulting from the work under this award.

Journal publications.

1. Riederer SJ, Borisch EA, Froemming AT, Grimm RC, Kawashima A, Mynderse LA, Trzasko JD, "Improved performance of prostate DCE-MRI using a 32-coil vs. 12-coil receiver array." Magn Reson Imaging 39:15-23 (2017).

2. Kargar S, Borisch EA, Froemming AT, Kawashima A, Mynderse LA, Stinson EG, Trzasko JD, Riederer SJ, "Robust and efficient pharmacokinetic parameter estimation for dynamic contrast enhanced MRI of the prostate," (in preparation).

Books or other non-periodical, one-time publications.
Nothing to Report

Other publications, conference papers and presentations.

1. Kargar S, Stinson EG, Borisch EA, Froemming AT, Kawashima A, Mynderse LA, Trzasko JD, Riederer SJ, "Patient-specific vs. population-based arterial input function in perfusion estimation for DCE-MRI of the prostate." Presented at 28th Annual Meeting of Society of Magnetic Resonance Angiography, Chicago IL, September 2016.

2. Kargar S, Borisch EA, Froemming AT, Kawashima A, Mynderse LA, Stinson EG, Trzasko JD, Riederer SJ, "Robust and efficient pharmacokinetic parameter estimation for dynamic contrast enhanced MRI of the prostate." Presented at 24th Annual Meeting, ISMRM, Honolulu HI, April 2017.

3. **Website(s) or other Internet site(s)**
Nothing to Report

4. **Technologies or techniques**
Nothing to Report

5. **Inventions, patent applications, and/or licenses**
Nothing to Report

6. **Other Products**
Nothing to Report

7. PARTICIPANTS & OTHER COLLABORATING ORGANIZATIONS

What individuals have worked on the project?

Name:	Stephen J. Riederer, Ph.D.
Project Role:	Principal Investigator
Nearest person month worked:	1.8
Contribution to Project:	Dr. Riederer directs all technical aspects of the projects.

Name:	Akira Kawashima, M.D., Ph.D.
Project Role:	Co-Investigator
Nearest person month worked:	.22
Contribution to Project:	Dr. Kawashima oversees feasibility testing performed in volunteers and provides feedback on intermediate results for all projects.

Name:	Eric A. Borisch
Project Role:	Information Services Technical Specialist
Nearest person month worked:	2.76
Contribution to Project:	Mr. Borisch is responsible for writing and developing production-level software for all projects, software heavily centered on reconstruction of 2D-accelerated 3D data sets acquired with various view orders.

Name:	Thomas C. Hulshizer
Project Role:	MR Technician
Nearest person month worked:	1.2
Contribution to Project:	Mr. Hulshizer is responsible for construction of the pelvis-prostate phantom, construction and tuning of RF coils, and testing of prototype MR pulse sequences using phantoms.

Has there been a change in the active other support of the PD/PI(s) or senior/key personnel since the last reporting period?

Stephen J. Riederer, Ph.D.
Ended February 2017
NIH R01 EB000212-27
"Modified Elliptical Centric View Orders for Improved Real-Time MRA" (PI: SJ Riederer, Ph.D.)
Purpose: develop image processing methods for estimating prostate perfusion parameters
3.6 months/year (30% effort)

What other organizations were involved as partners?

Nothing to Report other than the general support provided by the PI's institution, Mayo Clinic.

8. SPECIAL REPORTING REQUIREMENTS

None

9. APPENDICES: Attach all appendices that contain information that supplements, clarifies or supports the text. Examples include original copies of journal articles, reprints of manuscripts and abstracts, a curriculum vitae, patent applications, study questionnaires, and surveys, etc.

Manuscripts

Attached is a pdf copy of the published article:
"Improved Performance of Prostate DCE-MRI Using a 32-Coil vs. 12-Coil Receiver Array"

Magnetic Resonance Imaging 39 (2017) 15–23

Contents lists available at ScienceDirect

Magnetic Resonance Imaging

journal homepage: www.mrijournal.com

Original contribution

Improved performance of prostate DCE-MRI using a 32-coil vs. 12-coil receiver array

Stephen J. Riederer [a,*], Eric A. Borisch [a], Adam T. Froemming [a], Roger C. Grimm [a], Akira Kawashima [c], Lance A. Mynderse [b], Joshua D. Trzasko [a]

[a] Department of Radiology, Mayo Clinic, 200 First Street SW, Rochester, MN 55905, United States
[b] Department of Urology, Mayo Clinic, 200 First Street SW, Rochester, MN 55905, United States
[c] Department of Radiology, Mayo Clinic, 13400 E. Shea Blvd., Scottsdale, AZ 85259, United States

ARTICLE INFO

Article history:
Received 3 September 2016
Received in revised form 24 January 2017
Accepted 24 January 2017

Keywords:
Prostate MRI
DCE-MRI
Multi-element receiver coil

ABSTRACT

Purpose: To assess whether acquisition with 32 receiver coils rather than the vendor-recommended 12 coils provides significantly improved performance in 3D dynamic contrast-enhanced MRI (DCE-MRI) of the prostate.
Materials: The study was approved by the institutional review board and was compliant with HIPAA. 50 consecutive male patients in whom prostate MRI was clinically indicated were prospectively imaged in March 2015 with an accelerated DCE-MRI sequence in which image reconstruction was performed using 12 and 32 coil elements. The two reconstructions were compared quantitatively and qualitatively. The first was done using signal-to-noise ratio (SNR) and g-factor analysis to assess sensitivity to acceleration. The second was done using a five-point scale by two experienced radiologists using criteria of perceived SNR, artifact, sharpness, and overall preference. Significance was assessed with the Wilcoxon signed rank test. Extension to T2-weighted spin-echo and diffusion sequences was assessed in phantom studies.
Results: Reconstruction using 32 vs. 12 coil elements provided improved performance in DCE-MRI based on intrinsic SNR (18% higher) and g-factor statistics (14% higher), with a median 32% higher overall SNR within the prostate volume over all subjects. Reconstruction using 32 coils was qualitatively rated significantly improved ($p < 0.001$) vs. 12 coils on the basis of perceived SNR and radiologist preference and equivalent for sharpness and artifact. Phantom studies suggested the improvement in intrinsic SNR could extend to T2-weighted spin-echo and diffusion sequences.
Conclusions: Reconstruction of 3D accelerated DCE-MRI studies of the prostate using 32 independent receiver coils provides improved overall performance vs. using 12 coils.

1. Introduction

MR imaging of the prostate is commonly performed using a multiparametric approach in which multiple sequences are used to aid in radiologic interpretation [1–3]. In addition to T2-weighted spin-echo (T2SE) and diffusion-weighted image (DWI) a pulse sequence typically used within this exam is three-dimensional (3D) dynamic contrast-enhanced MRI (DCE-MRI) [4–6] in which a contrast agent is administered intravenously, and images are acquired of the prostate to observe washin and washout of the contrast-enhanced blood over the entire prostate volume. DCE-MRI continues to be used in the context of the PI-RADS version 2 reporting system for prostate cancer for treatment-naïve prostate glands [7]. Further, recurrence of prostate cancer after definitive treatment has been reported to be in the 15 to 40% range [8,9], and in such cases DCE-MRI has been shown to be of high value [10,11]. Because the desired spatiotemporal resolution of the DCE-MRI sequence typically pushes the limits of signal-to-noise ratio (SNR), the need for good performance of the receiver coils is important [12].

For prostate MRI the coil usage reported in the literature is highly variable. One significant choice is whether an endorectal (ER) coil should be used, and several studies have compared ER with non-ER acquisition [13–16]. However, whether an ER coil is used or not, in contemporary prostate MRI some kind of multi-element receiver coil is generally used. A sampling of the recent literature shows use of multi-element coils having four [17], six [18], eight [11,15,19], 12 to 15 [6], and 18 [20] elements, or with the number of elements not explicitly given [4,5].

For many contemporary MRI systems the number of receiver channels available is 32 or more. Also, coil arrays with literally dozens of elements are now embedded within the patient table. Although both of these factors can greatly facilitate the usage of a large number of elements for a

* Corresponding author.
E-mail addresses: riederer@mayo.edu (S.J. Riederer), borisch.eric@mayo.edu (E.A. Borisch), Froemming.Adam@mayo.edu (A.T. Froemming), Grimm.Roger@mayo.edu (R.C. Grimm), Kawashima.Akira@mayo.edu (A. Kawashima), Mynderse.Lance@mayo.edu (L.A. Mynderse), Trzasko.Joshua@mayo.edu (J.D. Trzasko).

http://dx.doi.org/10.1016/j.mri.2017.01.017
0730-725X/

given exam, it is not clear what the number or combination of elements should be for prostate MRI. If an ER coil is not used, then it is important to have a multicoil setup which provides high SNR in the region of the prostate. The results of Ref. [16] indicated superior performance for the combination of an ER coil and a 16-element multicoil vs. use of a six-element multicoil alone. However, separation of the improvement due to the change of the multicoil vs. use of the ER coil was not determined.

Prostate MRI at our institution is principally performed using a wide-bore 3 T MRI system with features similar to those described above. The vendor-recommended, default coil selection for prostate DCE-MRI calls for 12 channels of data acquisition to be used of the 32 available on the system. These 12 channels include eight active elements from the array contained within the table posterior to the supine patient and four active elements used from a 16-element array placed anteriorly. In investigating to what extent the DCE-MRI sequence could be accelerated, we considered whether additional coil elements could be used. To fully exploit the capability of the MRI system, the option for use of all 32 channels was considered. Thus, the specific hypothesis of this work was that the use of 32 vs. 12 independent receiver coils would provide improved performance in DCE-MRI of the prostate. The feasibility of improved performance for other sequences of a multi-parametric prostate MRI exam was also assessed with phantom studies.

2. Materials and methods

This study was approved by the institutional review board which waived the need for written consent. The study was compliant with HIPAA.

2.1. Subjects

50 consecutive male subjects for whom a prostate MRI exam was clinically indicated and who gave their assent for their exam results to be used for research purposes were prospectively enrolled in the study over the period March 10–27, 2015. The age, weight, and body mass index (BMI) ranges were 51 to 86 years, 63.5 to 155.1 kg, and 22.5 to 46.8, respectively. Forty-four of the 50 had intact prostates; six were evaluated post-prostatectomy. Other information on the patient cohort, including radiological interpretation, is shown in Table 1. Of note is that 34% (17/50) of the patients were imaged as followup to previous treatment for prostate cancer.

2.2. MRI acquisition

All studies were performed on either of two identical 3.0 T MRI scanners (Discovery MR750w, GE Healthcare, Waukesha WI) utilizing an institutional clinical exam protocol. Each machine has a 70 cm diameter bore, a vendor-provided 40-element receiver coil array (Geometry Embracing Method "GEM" array) embedded within the patient table, and 32 receiver channels. Each patient exam included a localizer, T2-weighted spin-echo, and diffusion-weighted sequences, followed by a DCE-MRI study performed with intravenous contrast administration. Details of the RF-spoiled gradient echo DCE-MRI sequence are shown in Table 2. Contrast material (Dotarem, Guerbet, Paris, France) was administered into an arm vein at a rate of 3 ml/s followed by a 20 ml saline flush at 3 ml/s. The contrast dose was 0.1 mmol/kg, with a maximum of 20 ml for patients weighing 100 kg or more.

The impetus for this study was to push the acceleration of the DCE-MRI sequence for improved spatiotemporal resolution. The sequence used is based on one developed for time-resolved contrast-enhanced MR angiography (CE-MRA) using two-dimensional (2D) SENSE acceleration [21] and view sharing [22]. For this work the slab orientation was approximately axial but with slight forward tilting to align the slab select direction with the central axis of the prostate gland as determined in the sagittal localizer. SENSE acceleration factors of 2.49 and 1.12 were applied along the left/right (L/R) phase encode and approximate superior/inferior (S/I) slice encode directions, respectively, yielding a net acceleration factor of $R = 2.78$. DCE-MRI acquisition was initiated 20 s prior to the start of contrast injection, the frame time was approximately 6.6 s, and a total of 33 time frames were collected. Versions of the sequence with higher accelerations were considered for shorter frame times; e.g. $R = 5.0$ for 4.0 s frame time, but for the same spatial resolution the SNR loss was considered too severe.

2.3. Selection of receiver coil elements

This work made use of the 40-element GEM receiver coil array shown schematically in Fig. 1A with a male torso and prostate shown approximately to scale. The array consists of five columns of elements oriented longitudinally within the patient table which for the supine patient are located posteriorly. Also used was a 16-element coil array placed anteriorly consisting of four longitudinally oriented columns each comprised of four elements (Fig. 1B). In both figures an approximate 75 cm^3 sphere, simulating the prostate gland, is shown in red to give a sense of scale of typical gland size to extent of coil coverage.

The combinations of coil elements available for usage are limited by the vendor, and recommendations are made according to the type of exam. For prostate MRI this calls for 12 active receiver coil elements, eight from the GEM array and four from the anterior array. These are highlighted in yellow in Figs. 1A and B, respectively. The elements selected from the GEM array (A) are the two central-most elements which encompass the S/I extent of the prostate, as identified from the sagittal scout images, and the three elements from the next closest columns on each side. For the anterior coil (B) the two central elements from the two rows which similarly encompass the S/I extent of the prostate are selected. All other coil elements from both arrays are electronically disabled during acquisition, and data from the 12 elements are individually digitized and used in reconstruction.

To attempt to exploit the full 32-channel capability of the MRI systems for accelerated DCE-MRI, we next considered use of the vendor-allowed 16 elements from each array. This is also depicted in Figs. 1A–B. Coil elements used for the 12-element case were expanded to include those shown in blue. For the GEM coil (A) the two central-most elements best aligned with the S/I prostate extent are selected as before.

Table 1
Summary of patient information and radiological interpretation. Interpretation was based on the full multi-parametric MRI exam, not just the DCE-MRI sequence.

Patients with no prior treatment	Number	Interpretation: *no suspicion of significant prostate cancer*	Interpretation: *suspicion of significant prostate cancer*
	33	16	17
Patients with prior treatment	Number	Interpretation: *no worrisome lesion*	Interpretation: *worrisome lesion*
Radical prostatectomy	6	2	4
Radiation therapy (external beam or brachytherapy, including with possible adjuvant hormonal therapy)	10	2	8
Hormonal therapy only	1	0	1
Total (patients with prior treatment)	17	4	13
Total (all patients)	50	20	30

Table 2
Parameters for 3D RF-spoiled gradient echo prostate DCE-MRI sequence. Acquisition of coil calibration images used the same sequence applied once with phase resolution reduced from 384 to 192.

Parameter	Value
Repetition time (TR)	5.3 msec
Echo time (TE)	2.2 msec
[a]Field of view	$220 \times 440 \times 114$ mm^3
[a]Sampling resolution	$256 \times 384 \times 38$
[a]Spatial resolution	$0.86 \times 1.15 \times 3.0$ mm^3
Acceleration	2.49 (R_Y) × 1.12 (R_Z) = 2.78
Frame time	6.6 s
Temporal footprint	≈19 s
Number of frames	33
Scan time	≈3.5 min

[a] These parameters are all expressed as (frequency × phase × slice) = (A/P × L/R × S/I).

The lateral rows containing those elements are supplemented with the rows of elements next positioned superiorly and inferiorly. For each row the leftmost and rightmost elements (e.g. elements 6 and 36 of Fig. 1A) are automatically combined in vendor hardware prior to digitization, in effect forming one virtual coil from two coil elements. Thus, the 20 elements contained within the four selected rows of the GEM coil are encoded in 16 individual coils, with four of these being two-element combinations. For the anterior array all 16 elements are used (B). It is noted that the channels used for the 12-coil acquisition are a subset of those used for the 32-coil reconstruction. The remaining 20 coil elements located at the ends of the GEM array are electronically disabled during the 32-coil acquisition.

2.4. Image reconstruction

Reconstruction was performed offline with standard SENSE unfolding [23] using a custom-built computing system described in [24]. To avoid the complications and potential variability of performing two separate DCE-MRI studies on each subject, we investigated if a single 32-coil acquisition could be done and the 12-coil acquisition accurately simulated by using only the appropriate 12 data sets for reconstruction. The risk with this approach is that the electronically active but unused 20 coil elements in the 32-active-element acquisition would interfere through undesirable coupling with the 12 elements selected for reconstruction. To assess this we first performed test scans in a volunteer in which separate acquisitions were done with the 12-active-coil and 32-active-coil approaches using the accelerated DCE-MRI sequence without contrast injection. Unaccelerated coil calibration image sets were also acquired with both approaches. Data from the 32-coil acquisition were reconstructed two ways: (i) using all 32 coils; and (ii) using data from only the same 12 coils as for the 12-active-coil acquisition. Reconstruction (iii) was done using all 12 coils of the 12-active-coil acquisition.

The images from reconstructions (i), (ii), and (iii) were compared in two ways. First, images of absolute SNR were formed from data sets (i), (ii), and (iii) using the method of Refs [25,26]. As the coil sensitivity profiles used in these calculations were estimated empirically via the root-sum-of-square demodulation, these SNR values are quantitatively approximate. Reconstructed SNR values were taken of a 3D volume just encompassing the prostate, in this case approximately 65 cm^3 and comprised of >20,000 pixels. Second, using the coil calibration data and assuming the acceleration factors of the DCE-MRI sequence in Table 2, images were formed of the g-factor, a mathematical measure of the ability of a receiver coil array to retain SNR in accelerated MR acquisition [23]. These comparisons, shown in Fig. 2, indicated that the SNR (A) and g-factor statistics (B) of reconstructions (ii) and (iii) were essentially indistinguishable, and both were different from results for reconstruction (i). Consequently, results for the 12-coil reconstruction were generated in the patient study by selecting data only from those 12 elements from the 32-active-coil acquisition and reconstructing that data. Comparisons were then made with the reconstruction using the full 32-coil data set.

2.5. Radiological evaluation

For each of the 50 patient studies the 32-coil DCE-MRI sequence was reconstructed, and images were zero padded by a factor of 2 and cropped to effectively magnify the region surrounding the prostate. An observer not performing the radiological evaluation selected an axial partition midway through the S/I extent of the prostate at the time frame closest to 50 s post injection. This typically corresponded to a time 10 to 20 s after peak contrast enhancement of any rapidly enhancing lesions in the prostate. The magnified 32-coil and 12-coil images from this partition and time frame were then placed side-by-side randomly and in blinded fashion for each study. This set of 50 composite images was then provided to each reviewer.

The two radiologist reviewers (ATF, six years' experience in prostate MRI; AK, 20 years' experience) then independently graded each image pair using a five-point scale (-2 = left (L) image significantly better than right (R) image; -1 = L slightly better than R; 0 = L and R images equivalent; $+1$ = R slightly better than L; $+2$ = R significantly better than L). This was done for each of the four criteria of perceived SNR, level of artifact, sharpness, and overall preference.

In addition, images of absolute SNR were made for the 32-coil and 12-coil reconstructions for each of the studies using the coil calibration images as described previously for the volunteer study. For this analysis images from the six of the 50 patients who were imaged post-prostatectomy were excluded. For each study the 3D rectangular volume was identified on the reconstructed images which just encompassed the prostate, histograms of the SNR values were generated for all voxels within the volume for the two reconstructions, and the ratio of median values of the 32-coil vs. 12-coil histograms was taken as a measure of SNR improvement for that study. These volumes ranged from 28 to 265 cm^3 with a median of 101 cm^3, typically including several tens of thousands of pixels. This process was repeated for the g-factor for the acceleration used in the DCE-MRI run, and the ratio of median g-factor values determined.

2.6. Statistical significance

For the radiological evaluation after accounting for the blinded presentation, significant (defined as $p < 0.05$) difference from the null hypothesis of equivalent performance was assessed with the Wilcoxon signed rank test.

2.7. Extension to other pulse sequences for prostate MRI

After having demonstrated improved performance in prostate DCE-MRI, it was of interest to assess potential improvement in the other sequences of multi-parametric prostate MRI, namely T2-weighted spin-echo (T2SE) and diffusion-weighted imaging (DWI). This was not possible with the 50 patient studies described previously. To study this in a controlled manner a phantom was used, consisting of a plastic, male-like pelvic shell filled with B-gel, sorbic acid, and salt dissolved in water which upon congealing mimics soft tissue. During the pouring two inclusions were added, one a 50 cm^3 balloon to mimic the bladder and the second a 40 cm^3 balloon to mimic the prostate. For both balloons the B-gel concentration was adjusted to provide slight but discernible signal differences vs. background. A photograph of the phantom is shown in Fig. 8A. Based on phantom size, it corresponds to a BMI of approximately 24.

The phantom was imaged with the 12- and 32-coil arrangements using the sequences: (i) DCE-MRI described above, (ii) coronal T2SE, (iii) full lateral-FOV "conventional" axial DWI, and (iv) limited-lateral-FOV axial DWI [27]. Sequence parameters are shown in Table 3. The

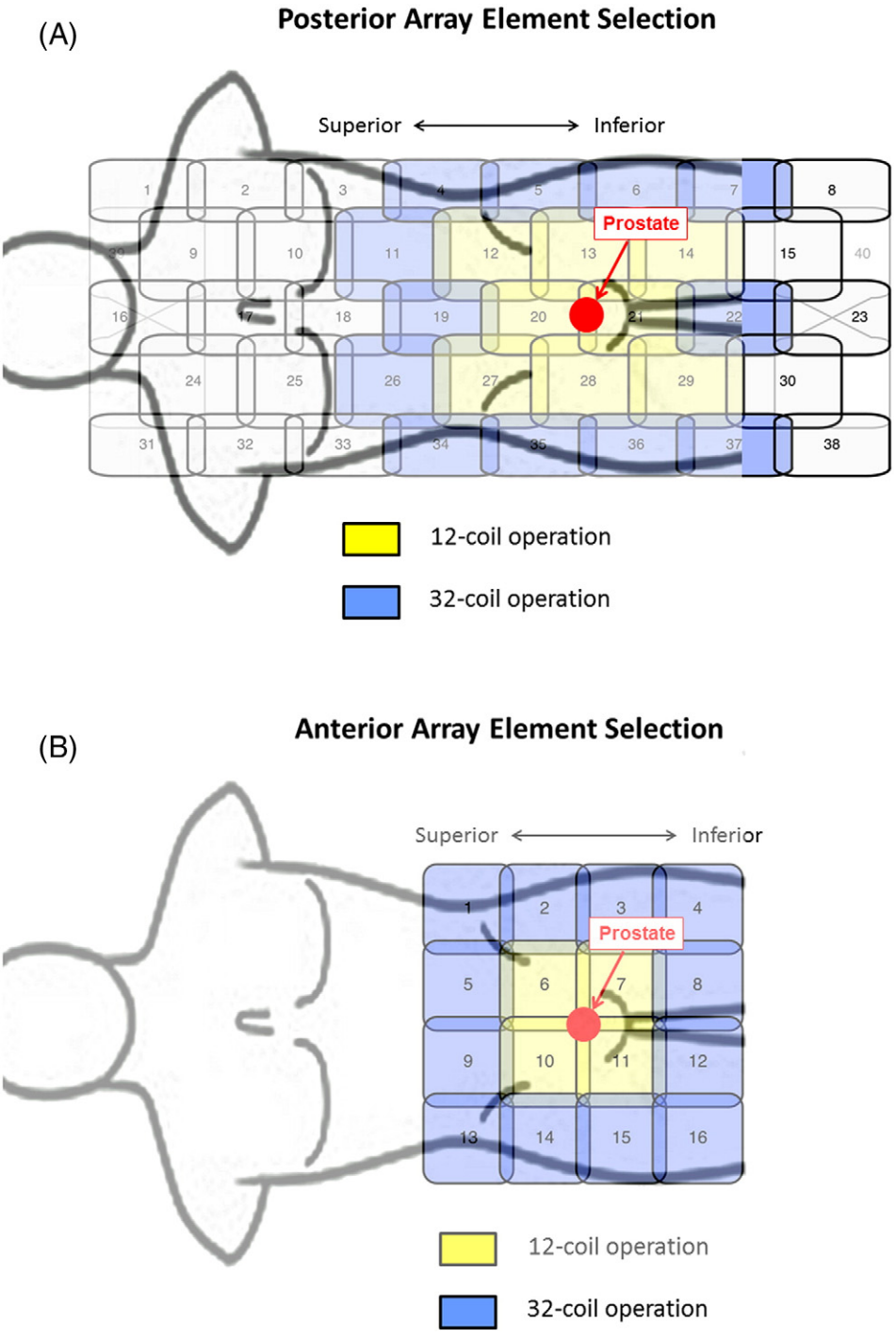

Fig. 1. Schematics of coil elements and element selection for 12-coil and 32-coil operation. (A) 40-element GEM array contained within the patient table and located posterior to the supine patient. (B) Schematic of 16-element array placed anteriorly to the supine patient. For 12-channel operation the coil elements shown in yellow are selected, eight from the posterior array and four from the anterior array. For 32-channel operation all coils in yellow and additionally those in blue are selected. For the posterior GEM array signals from the lateral-most elements are paired (4 with 34, 5 with 35, etc.) and combined in hardware into one virtual coil per pair. For 32-channel operation all 16 elements of the anterior array are used.

DCE-MRI data was used to reconstruct 3D images of absolute SNR as described previously, and the ratio between the 32- vs. 12-coil images taken as a measure of absolute intrinsic SNR improvement. Each of the other sequences was run twice, the same gain settings for both runs. For each sequence an image from one of the runs was selected of a section midway through the prostate inclusion. The signal S was taken as the mean over a circular, approximate 2 cm^2 region-of-interest (ROI) within the inclusion. Noise σ was assessed by forming the difference image between the two acquired images of the same anatomic section, measuring the standard deviation in the same ROI as used for signal, and dividing the result by $\sqrt{2}$ to account for the subtraction. SNR was then defined as S/σ, and the ratio of SNRs of 32- and 12-coil acquisition determined.

3. Results

Fig. 2B shows the cumulative histograms of the g-factor values for the 32-coil and 12-coil reconstructions. The solid green, blue, and red

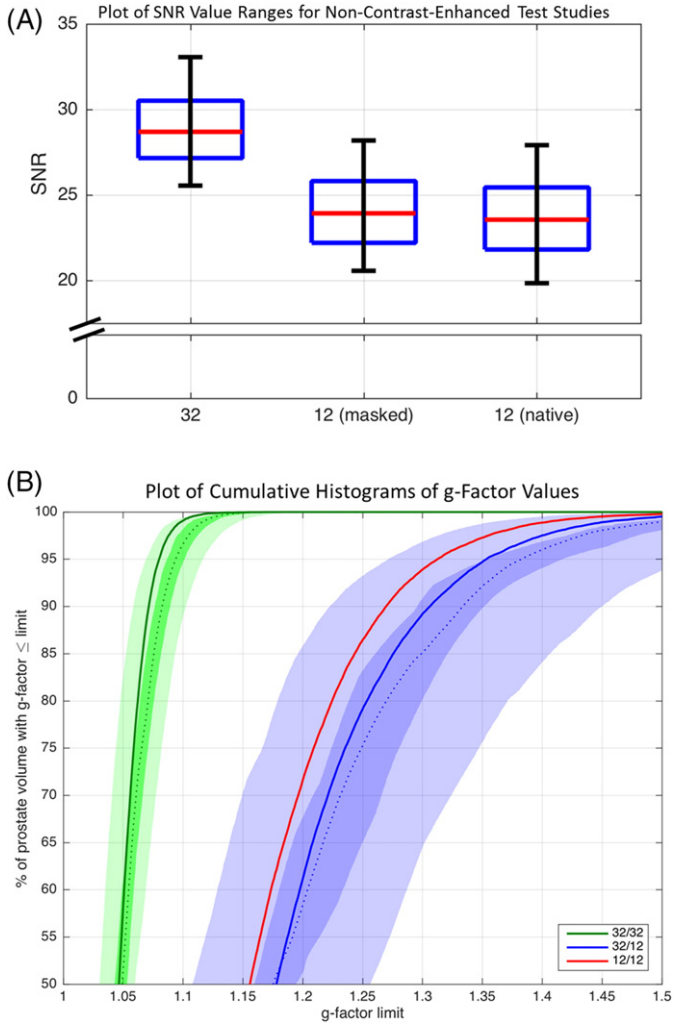

Fig. 2. (A) Box and whisker plots of the reconstructed SNR values from the non-contrast-enhanced test case evaluating reconstructions (i) 32-coil acquisition with 32-coil reconstruction, (ii) 32-coil acquisition with 12-coil reconstruction ("masked"), and (iii) 12-coil acquisition with 12-coil reconstruction ("native"). Each figure shows the median, ±25% values (box boundaries), and ±45% boundaries (whiskers). Median values are 28.7, 23.9, and 23.5 (a.u.). (B) Plot of the cumulative g-factor statistics for the 32-channel acquisition with 32-coil (green lines and curves) and 12-coil (blue lines and curves) reconstructions and for the 12-channel acquisition with 12-coil reconstruction (solid red line). The three solid curves are for the non-contrast-enhanced test scans. The shaded green and blue zones show the ranges of g-factor values measured across the 32-coil and 12-coil reconstructions for all 50 patient studies, respectively. The dotted green and blue lines correspond to the median values, the dark shaded zones to ±12.5% about the median and the light shaded zones to ±37.5% about the median. For all plots the statistics are measured over the 3D volume encompassing the prostate.

lines are for the unenhanced test scans of the volunteer. The green shaded region shows the cumulative g-factor histogram for the 32-coil reconstruction based upon all 50 patient studies. The dashed green line is the median value; the dark green zone encompasses the central 25%, and the light green zone the central 75% at that cumulative percentage. Similarly, the blue shaded region shows analogous results for the 12-coil reconstruction. The more rapid approach to 100% of the green 32-coil reconstruction indicates the overall smaller g-factor values and better retention of SNR vs. the two 12-coil reconstructions (blue curves and blue regions and red curve). This distinction between curves is maintained across all 50 patient studies in that the shaded green and blue regions are well separated. The close match of the blue regions and red curve indicates the equivalence in performance of reconstruction (ii) and (iii).

Fig. 3 shows results from the qualitative evaluation of the two radiologists. 32-coil reconstruction (positive scores) was evaluated as

Table 3
Technical parameters of T2SE and DWI pulse sequences used for phantom-based SNR analysis.

Parameter	T2SE	Conventional DWI	Limited-FOV DWI
Format	Coronal	Axial	Axial
Field of View (mm^2) ($FOV_X \times FOV_Y$)	220 × 220	360 × 360	260 × 130
Acquisition matrix (X × Y)	320 × 320	192 × 192	144 × 72
Inplane resolution (mm^2) (X × Y)	0.688 × 0.688	1.875 × 1.875	1.8 × 1.8
Slice Thickness/spacing (mm for both)	3/3.3	3/0	4/0
TR (ms)	4951	5888	3925
TE (ms)	96	70	75
Number of slices	26	23	16
b-Values (s/mm^2)	–	100/1000	100/1000
Number of averages	1	1	1

The T2SE sequence used a fast-spin-echo readout with an echo train length of 4.

significantly superior ($p < 0.001$) to 12-coil reconstruction using the criteria of SNR (A) and overall preference (D) by both reviewers individually and in aggregate. 32-coil and 12-coil reconstructions were evaluated as equivalent for the criteria of level of artifact (B) and sharpness (C) by both reviewers individually and in aggregate. For perceived SNR the two reviewers' scores matched in 38/50 cases and were within one value on the five-point −2 to +2 scale in all 50/50. For artifact these corresponding results were 34/50 and 50/50; for sharpness 27/50 and 46/50; for overall preference 22/50 and 47/50.

Fig. 4 shows the percent improvement in SNR values provided by the 32-coil vs. 12-coil reconstruction plotted vs. the BMI of the patient. The red circles show the case with no acceleration, as determined from the images of SNR using the coil calibration data. The median increase (18%) over the 44 studies is noted with the red hashmark on the ordinate axis, and the trend line, determined by least squares regression,

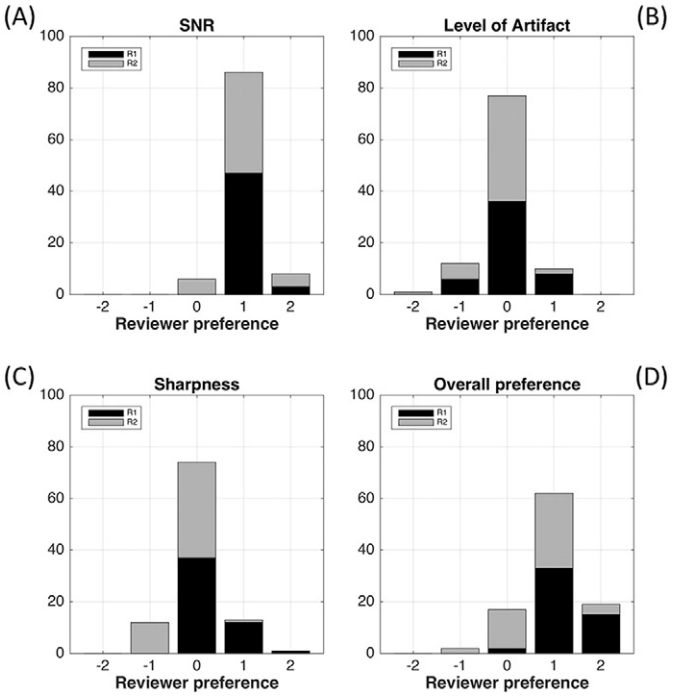

Fig. 3. Histograms showing the results of the radiological review for perceived SNR (A), level of artifact (B), sharpness (C), and overall preference (D). For SNR (A) and overall preference (D) the preference for the 32-coil reconstruction (positive scores) was significant ($p < 0.001$) for both reviewers individually and in aggregate. For artifact (B) and sharpness (C) there was no significant preference.

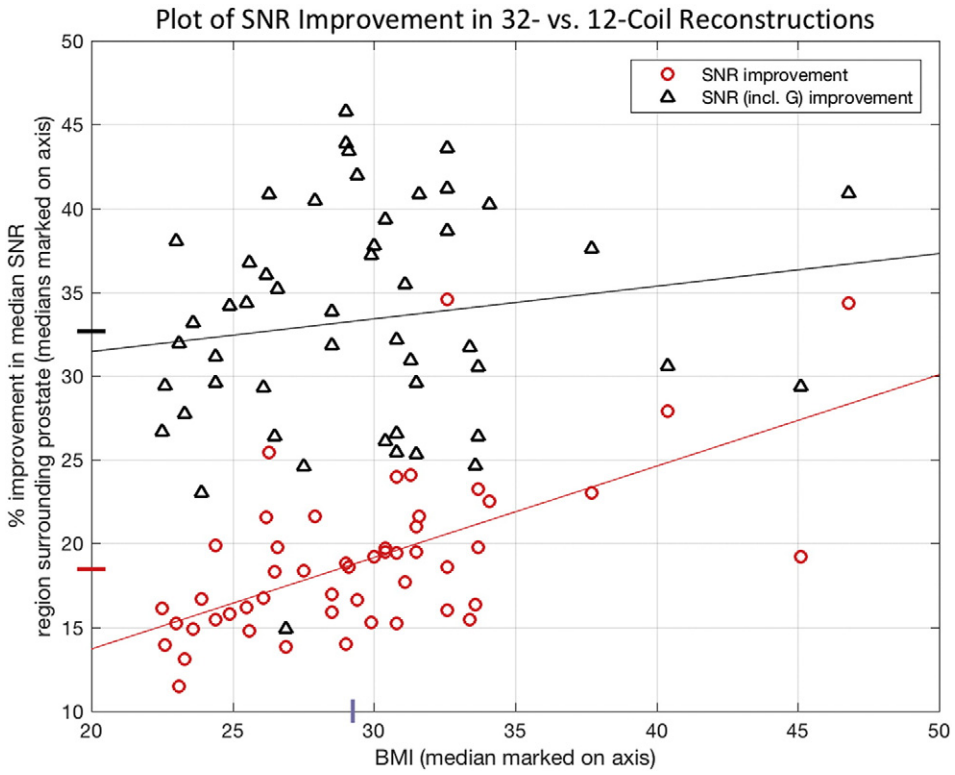

Fig. 4. Plot of the ratio of median reconstructed SNR values without (red circles) and with (black triangles) the additional effect of g-factor improvements for the 32-coil and 12-coil reconstructions plotted vs. BMI of the patient. In each case values were computed from a volume encompassing the prostate. The median increase for each is shown in the corresponding colored hashmark on the ordinate, and trend lines of each with BMI, as determined from least square regression, are also noted.

shown in red. The triangles show the case when acceleration is additionally used at the acceleration factors employed in this study with analogous median (32%) and trend lines shown in black. The median BMI (29.1) for the 50 studies is also noted as a hashmark on the abscissa.

Figs. 5-7 show sample results from three patient studies in which the 32-coil and 12-coil reconstructions are compared. Video V1 compares all 31 time frames for 12- vs. 32-coil reconstructions for the study presented in Fig. 5.

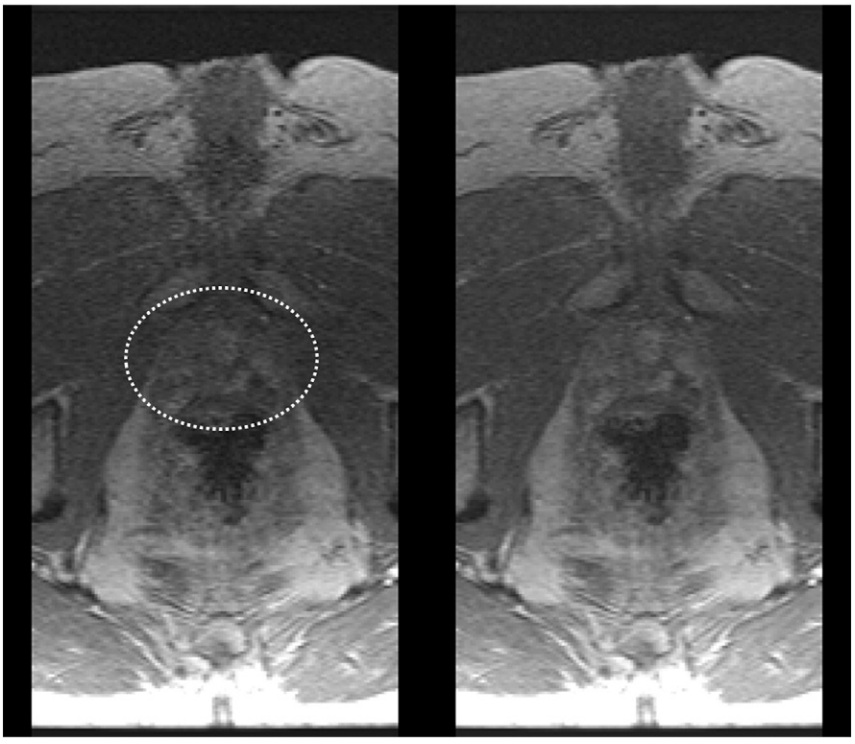

Fig. 5. Comparison of 12-coil (left) and 32-coil (right) reconstructions of prostate DCE-MRI in a patient with BMI 26.6. Prostate is identified within the white ellipse. Radiologists #1 and #2 both assigned scores of (+2, 0, 0, +2) for (perceived SNR, artifact level, sharpness, overall preference) where positive scores reflect preference for the 32-coil result.

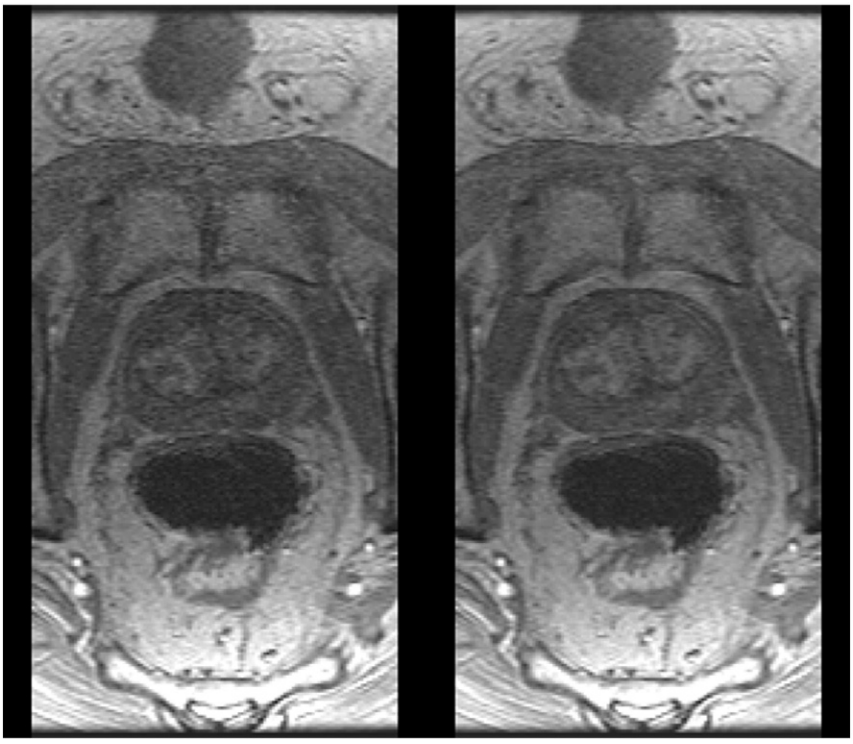

Fig. 6. Comparison of 12-coil (left) and 32-coil (right) reconstructions of prostate DCE-MRI in a patient with BMI 30.4. Radiologists #1 and #2 assigned scores of (+1, 0, 0, +1) and (+1, 0, 0, +2).

Table 4 summarizes results for relative SNR for the phantom studies which show an SNR increase ranging from 9.7% for T2SE to 34.3% for the b-1000 conventional DWI. Fig. 8B is a axial image of the phantom showing the SNR increase determined from the DCE-MRI coil calibration data. The position of the prostate inclusion is designated by the dashed circle. Fig. 8C is a side-by-side comparison of unsubtracted coronal T2SE images of the phantom using 12- (left) and 32-coil (right) acquisition illustrating the size and placement of the bladder and prostate inclusions.

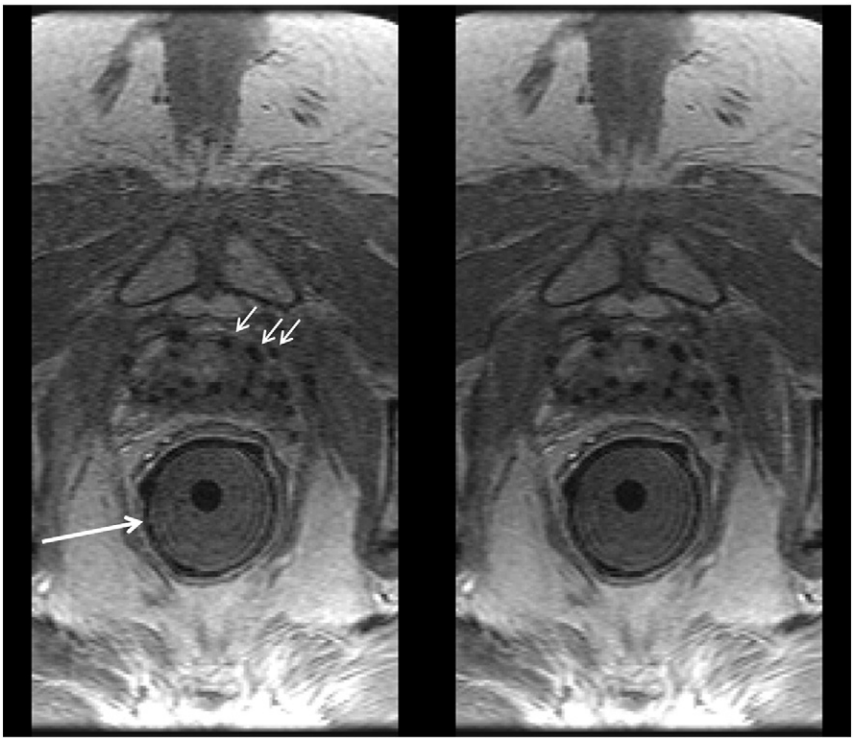

Fig. 7. Comparison of 12-coil (left) and 32-coil (right) reconstructions of prostate DCE-MRI in a patient with BMI 33.4 and with implanted seeds for brachytherapy (black dropouts, e.g. short white arrows). In this exam an endorectal coil used for sequences other than DCE-MRI was applied within a gel-filled insert (long white arrow) but not active for the DCE-MRI sequence. Radiologists #1 and #2 assigned scores of (+1, 0, 0, +1) and (0, 0, 0, 0).

Table 4
Relative SNR of 32- vs. 12-coil acquisition as measured in prostate phantom.

Comparison	Sequence	Relative SNR
1	T2SE	1.097
2	Conventional DWI ($b = 100$ s/mm^2, 1 average)	1.163
3	Conventional DWI ($b = 1000$ s/mm^2, 1 average)	1.346
4	Limited-FOV DWI ($b = 100$ s/mm^2, 1 average)	1.116
5	Limited-FOV DWI ($b = 1000$ s/mm^2, 1 average)	1.338

4. Discussion

For the same level of acceleration, the acquisition and reconstruction of data from 32 receiver coils encompassing the pelvis provides superior measured and perceived SNR in dynamic-contrast-enhanced prostate MRI vs. use of the vendor-recommended 12 receiver coils. The median improvement in overall measured SNR was 32% over the volume of the prostate. Although the placement of the 12 receiver elements used already encompasses the full lateral and superior/inferior extent of the prostate, the incorporation of data from additional coils can provide improved performance without generation of artifact related to the increase in number of elements.

There are possible disadvantages in the use of additional receiver coils in image reconstruction. When done on the vendor system, the reconstruction time for a 32-coil DCE-MRI run is 50 s vs. 15 s on our custom hardware. Lacking high speed computational hardware, reconstruction time can possibly be reduced by grouping coil elements together before digitization to reduce the overall number of data channels [28,29]. However, as commercial systems continue to improve in the future, reconstruction times are expected to decrease and make this less of an issue.

Another possible disadvantage in the use of incremental coils located somewhat distantly from the FOV of interest is that motion of distant objects might alias into the reconstructed FOV owing to the high sensitivity of the incremental coils to the moving object. The evaluation performed in this work indicated that this was not a significant problem. If artifact were present and could be associated with some specific distant body region, then conceivably the reconstruction could be repeated with data from the coils nearby to that region excluded.

In this work data from each 32-coil DCE-MRI acquisition were reconstructed two ways, the first using all 32 coils and the second using only 12 coils, and the results compared. This study design eliminated the additional uncertainty and expense associated with a study in which each subject would have been imaged twice with contrast material, once with each coil set. We validated this approach by comparing 12-coil reconstruction from 32- and 12-coil acquisitions and showed negligible difference in SNR and g-factor.

This study evaluated two vendor-provided configurations of the coil arrays available with the MRI system. It is possible that other configurations might provide improved performance. Specifically, acceleration applied along a particular direction benefits from coil elements which tend to face each other along that direction. Electrically combining the two most lateral elements of the GEM array into one virtual coil, as done by the vendor, might not be optimal for this array for L/R acceleration. Also, other styles of receiver coil arrays may provide improved performance, such as arrays placed in better proximity or wrapped around the pelvis. Incorporation of an endorectal coil can be expected to provide some improvement in SNR near that coil. In this work although an endorectal coil was placed in some subjects as seen in Fig. 7, it was active only for sequences other than DCE-MRI.

The quantitative analysis distinguished between SNR improvement solely due to the increase in the number of coils in an unaccelerated scan (red dots of Fig. 4) as well as that due to improvement in g-factor

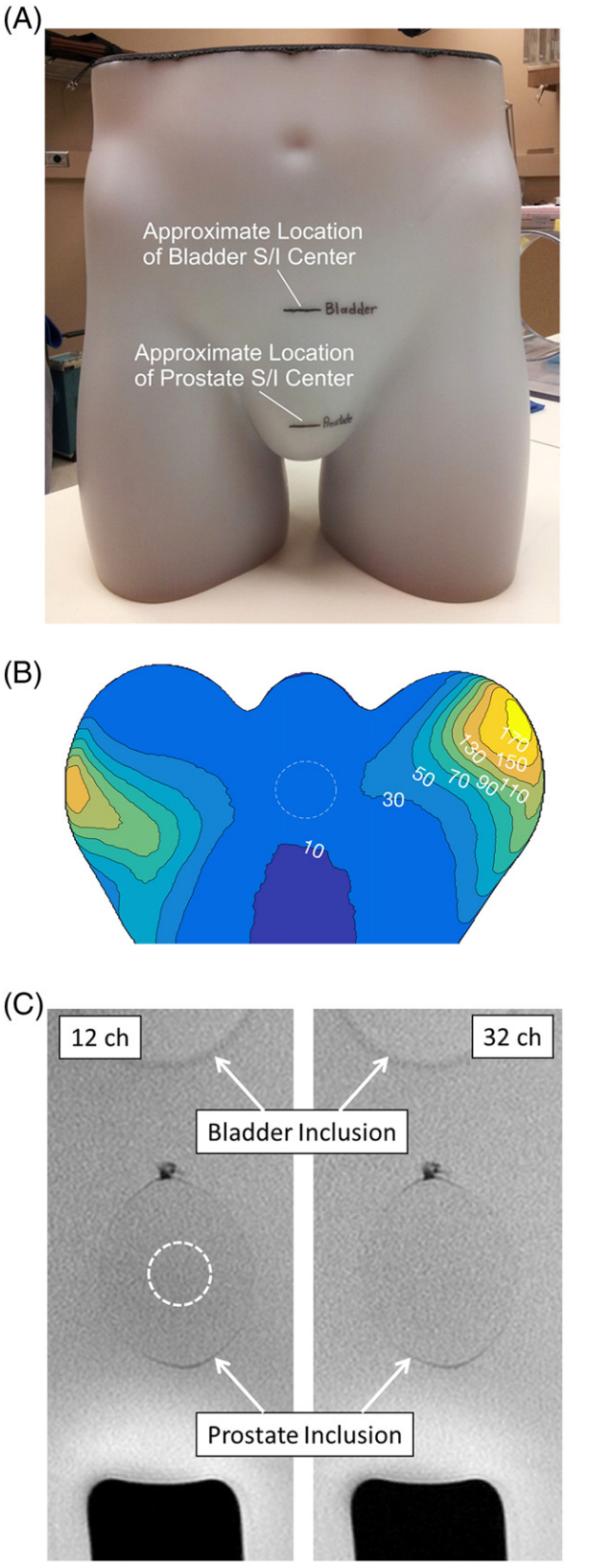

Fig. 8. (A) Photograph of phantom used for assessment of prostate MRI. Superior/inferior levels of bladder and prostate inclusions are noted. (B) Axial image of the phantom at the level of prostate inclusion (dashed circle) showing relative percent improvement in SNR of 32- vs. 12-coil acquisition. (C) Coronal T2SE images of the phantom acquired using 12- (left) and 32-coil (right) acquisitions. The observed 9.7% SNR increase is difficult to visualize, but the images show the size and location of the prostate inclusion. ROI used for SNR measurement is indicated as dashed ellipse (left image).

statistics (increment between red dot and black triangle for each patient) at the specific acceleration factor used. The first of these should benefit any sequence. The 32-coil array provided improvement in both SNR and in g-factor statistics vs. the 12-coil array. Both are important in acquisitions such as DCE-MRI in which acceleration is used. It is interesting that the level of improvement of SNR (red circles of Fig. 4) appeared to correlate positively with BMI.

Extending this to sequences beyond DCE-MRI, the phantom study results in Table 4 indicate that both T2SE and DWI are expected to benefit with improved SNR with 32-coil acquisition. Consistent with the results shown, sequences which are particularly signal-starved, such as high-b value DWI, might in practice benefit more from the SNR increase. This can potentially be used to reduce the level of averaging commonly done in DWI.

The benefit of increased SNR can be used for DCE-MRI in various ways. As stated, we initially investigated but opted not to go to faster frame rates. We have developed a version for assessment of biochemical recurrence with higher spatial resolution ($0.76 \times 0.87 \times 2.24$ mm^3 vs. the $0.86 \times 1.15 \times 3.0$ mm^3 of this work) with a 15 s vs. 6.6 s frame time.

In addition to the above-described extended reconstruction time and possible motion artifact from distant objects, another limitation of this work is that further study is necessary to determine whether prostate lesion detection and characterization are improved with 32-coil DCE-MRI. Also, study of the impact in T2SE and DWI sequences should be extended to a detailed patient series for a more complete assessment.

In summary, for the same level of acceleration, the acquisition and reconstruction of data from 32 receiver coils encompassing the pelvis provides superior measured and perceived SNR in dynamic-contrast-enhanced prostate MRI vs. use of 12 receiver coils.

Supplementary data to this article can be found online at http://dx.doi.org/10.1016/j.mri.2017.01.017.

Funding

NIH EB000212, EB017840, RR018898; DOD W81XWH-15-1-0341; NSF CIF:1818347.

Acknowledgments

We acknowledge the assistance of Brent A. Warndahl in performing the studies.

References

[1] Delongchamps NB, Rouanne M, Flam T, et al. Multiparametric magnetic resonance imaging for the detection and localization of prostate cancer: combination of T2-weighted, dynamic contrast-enhanced and diffusion-weighted imaging. BJU Int 2010;107:1411–8.
[2] Dickinson L, Ahmed HU, Allen C, et al. Magnetic resonance imaging for the detection, localization, and characterization of prostate cancer: recommendations from a European consensus meeting. Eur Urol 2011;59:477–94.
[3] Barentz JO, Richenberg J, Clements R, et al. ESUR prostate MR guidelines 2012. Eur Radiol 2012;22:746–57.
[4] Franiel T, Hamm B, Hricak H. Dynamic contrast-enhanced magnetic resonance imaging and pharmacokinetic models in prostate cancer. Eur Radiol 2011;21:616–26.
[5] Verma S, Turkbey B, Muradyan N, et al. Overview of dynamic contrast-enhanced MRI in prostate cancer diagnosis and management. AJR 2012;198:1277–88.
[6] Rosenkrantz AB, Geppert C, Grimm R, et al. Dynamic contrast-enhanced MRI of the prostate with high spatiotemporal resolution using compressed sensing, parallel imaging, and continuous golden-angle radial sampling: preliminary experience. J Magn Reson Imaging 2015;41:1365–73.
[7] Weinreb JC, Barentsz JO, Choyke PL, et al. PI-RADS prostate imaging - reporting and data system: 2015, version 2. Eur Urol 2016;69:16–40.
[8] Han M, Partin AW, Zahurak M, Piantadosi S, Epstein JI, Walsh PC. Biochemical (prostate specific antigen) recurrence probability following radical prostatectomy for clincally localized prostate cancer. J Urol 2003;169:517–23.
[9] Trock BJ, Han M, Freedland SJ, et al. Prostate cancer-specific survival following salvage radiotherapy vs. observation in men with biochemical recurrence after radical prostatectomy. JAMA 2010;299:2760–9.
[10] Rouviere O, Vitry T, Lyonnet D. Imaging of prostate cancer local recurrences: why and how? Eur Radiol 2010;20:1254–66.
[11] Kitajima K, Hartmann RP, Froemming AT, Hagen CE, Takahashi N, Kawashima A. Detection of local recurrence of prostate cancer after radical prostatectomy using endorectal coil MRI at 3 T: addition of DWI and dynamic contrast enhancement to T2-weighted MRI. AJR 2015;205:807–16.
[12] Attenberger UI, Ingrisch M, Dietrich O, et al. Time-resolved 3D pulmonary perfusion MRI: comparison of different k-space acquisition strategies at 1.5 and 3 T. Invest Radiol 2009;44:525–31.
[13] Park BK, Kim B, Kim CK, Lee HM, Kwon GY. Comparison of phased-array 3.0-T and endorectal 1.5-T magnetic resonance imaging in the evaluation of local staging accuracy for prostate cancer. J Comput Assist Tomogr 2007;31(4):534–8.
[14] Heijmink SW, Futterer JJ, Hambrock T, et al. Prostate cancer; body-array versus endorectal coil MR imaging at 3 T - comparison of image quality, localization, and staging performance. Radiology 2007;244(1):184–95.
[15] Mazaheri Y, Vargas HA, Nyman G, Shukla-Dave A, Akin O, Hricak H. Diffusion-weighted MRI of the prostate at 3.0 T: comparison of endorectal coil (ERC) and phased-array coil (PAC) MRI - teh impact of SNR on ADC measurement. Eur J Radiol 2013;82:e515–20.
[16] Turkbey B, Merino MJ, Gallardo EC, et al. Comparison of endorectal coil and nonendorectal coil T2 W and diffusion-weighted MRI at 3 Tesla for localizing prostate cancer: correlation with whole-mount histopathology. J Magn Reson Img 2014;39:1443–8.
[17] Hotker AM, Mazaheri Y, Aras O, et al. Assessment of prostate cancer aggressiveness by use of the combination of quantitative DWI and dynamic contrast-enhanced MRI. AJR 2016;206:756–63.
[18] Ocak I, Bernardo M, Metzger G, et al. Dynamic contrast-enhanced MRI of prostate cancer at 3 T: a study of pharmokinetic parameters. AJR 2007;189:W192–201.
[19] Fennessy FM, Fedorov A, Penzkofer T, et al. Quantitative pharmokinetic analysis of prostate cancer DCE-MRI at 3 T: comparison of two arterial input functions on cancer detection with digitized whole mount histopathological validation. Magn Reson Img 2015;33:886–94.
[20] Cho E, Chung DJ, Yeo DM, et al. Optimal cut-off value of perfusion parameters for diagnosing prostate cancer and for assessing aggressiveness associated with Gleason score. Clinical Img 2015;39:834–40.
[21] Haider CR, Hu HH, Campeau NG, Huston III J, Riederer SJ. 3D high temporal and spatial resolution contrast-enhanced MR angiography of the whole brain. Magn Reson Med 2008;60:749–60.
[22] Riederer SJ, Tasciyan T, Farzaneh F, Lee JN, Wright RC, Herfkens RJ. MR fluoroscopy: technical feasibility. Magn Reson Med 1988;8:1–15.
[23] Pruessmann KP, Weiger M, Scheidegger MB, Boesiger P. SENSE: sensitivity encoding for fast MRI. Magn Reson Med 1999;42:952–62.
[24] Borisch EA, Trzasko JD, Froemming AT, et al. Faster-than-acquisition 4D sparse reconstruction for Cartesian 2D SENSE-type acquisition. 23rd Annual Mtg. Toronto: ISMRM; 2015. p. 1580.
[25] Kellman P, McVeigh ER. Image reconstruction in SNR units: a general method for SNR measurement. Magn Reson Med 2005;54:1439–47.
[26] Kellman P, McVeigh ER. Erratum to Kellman P, McVeigh ER. Image reconstruction in SNR units: a general method for SNR measurement. Magn Reson Med 2005;54:1439–1447. Magn Reson Med 2007;58:211–2.
[27] Feng Z, Min X, Kumar Sah V, et al. Comparison of field-of-view (FOV) optimized and constrained undistorted single shot (FOCUS) with conventional DWI for the evaluation of prostate cancer. Clinical Img 2015;39:851–5.
[28] Buehrer M, Pruessmann KP, Boesiger P, Kozerke S. Array compression for MRI with large coil arrays. Magn Reson Med 2007;57:1131–9.
[29] Beatty PJ, Chang S, Holmes JH, et al. Design of k-space channel combination kernels and integration with parallel imaging. Magn Reson Med 2014;71:2139–54.